machines

MDPI

Article

Study on a Fully Electrified Steering System and Its Control Strategies for Heavy-Duty Wheeled Platforms

Shicheng Zheng [1,2], Tianxiang Qin [1], Jingkun Wei [3], Jiaming Cheng [4], Xiaming Yuan [1,2,*] and Jihong Zhu [1,2,*]

[1] Department of Precision Instrument, Tsinghua University, Beijing 100084, China; shichengzhengs@mail.tsinghua.edu.cn (S.Z.); qtx22@mails.tsinghua.edu.cn (T.Q.)
[2] State Key Laboratory of Precision Space-Time Information Sensing Technology, Qinghua Garden, Chengfu Road, Haidian District, Beijing 100084, China
[3] School of Mechanical Engineering and Automation, Beihang University, 37 Xueyuan Road, Haidian District, Beijing 100191, China; weijingkun@buaa.edu.cn
[4] College of Mechanical and Electrical Engineering, Huangshan University, Huangshan 245041, China; 112601@hsu.edu.cn
* Correspondence: xmyuan@mail.tsinghua.edu.cn (X.Y.); jhzhu@tsinghua.edu.cn (J.Z.)

Abstract

To address the limitations of the centralized hydraulic steering system used in the first-generation heavy-duty wheeled platform developed by our team, this study proposes a fully electrified steering system based on a compact direct-drive electro-mechanical actuator (DEMA) architecture. Compared with the original hydraulic system, the proposed solution reduces the steering-system weight from approximately 150 kg to 32 kg in the single-channel configuration and 40 kg in the dual-channel configuration, while significantly improving system integration and maintainability. For the single-channel DEMA steering system, a composite control strategy combining three-loop PID control with feedforward compensation is developed to improve dynamic response and position-tracking accuracy. AMESim simulation results under a steering resistance torque of 6000 $\pm$ 500 Nm show that the system achieves an overshoot below 2%, a steady-state error below 0.1°, and a tracking error below 0.4°. To reduce motor power and thermal-management requirements, a dual-channel DEMA steering architecture is further proposed. Considering inter-channel parameter differences, a primary–secondary synchronization control strategy is developed to suppress force-fighting behavior and improve motion consistency. Simulation results demonstrate that the proposed strategy effectively reduces synchronization errors and maintains highly consistent force output between channels while preserving excellent steering accuracy and tracking performance. The proposed fully electrified steering system and synchronization control strategy provide an effective solution for improving the dynamic performance, lightweight design, and reliability of heavy-duty wheeled platforms.

Keywords: heavy-duty wheeled platform; steering system; direct-drive electro-mechanical actuator (DEMA); composite control strategy; primary–secondary synchronization control strategy

Check for updates

Academic Editor: Tamara Nestorović

Received: 21 April 2026
Revised: 27 May 2026
Accepted: 10 June 2026
Published: 12 June 2026

Copyright: © 2026 by the authors. Licensee MDPI, Basel, Switzerland. This article is an open access article distributed under the terms and conditions of the Creative Commons Attribution (CC BY) license.

1. Introduction

With continuous advances in perception, artificial intelligence, electromechanical technology, and automation, unmanned special-purpose equipment has experienced rapid development. Benefiting from advantages such as remote operability, rapid deployment, high integration, strong autonomy, broad environmental adaptability, cost-effectiveness,

good concealment, and reduced risks to warfighters, such equipment has been widely adopted worldwide and is reshaping modern battlefields.

Heavy-duty unmanned mobile platforms are crucial assets for performing diverse missions, including reconnaissance, surveillance, and fire support on the future battlefield. As a key component of integrated sea–land–air–space operational systems, their large-scale deployment on the future battlefield will not only enhance coordination among combat units but also exert a profound impact on combat patterns and modes of warfare. A high-performance unmanned wheeled platform should be capable of operating in complex environments, among which the steering system serves as a core component for direction control and path tracking. An advanced steering system should feature a compact structure, ease of maintenance, and excellent dynamic performance to ensure good maneuverability and control precision of the heavy-duty unmanned wheeled platform in challenging conditions. In recent years, the stability control technologies [1–9] and composite rapid steering technologies [10–17] for unmanned wheeled platforms have received increasing research attention. The effectiveness of these technologies fundamentally depends on the excellent performance of the steering system, while improved structural design and dynamic characteristics of the steering system are essential prerequisites for achieving enhanced steering stability and rapid response.

As performance requirements for heavy-duty unmanned wheeled platforms continue to rise, their steering systems should deliver higher output torque to meet manipulation demands under complex working conditions. To address the limitations of single-channel actuators in providing sufficient torque, dual-actuator configurations are commonly adopted to jointly drive the steering mechanism. However, motion asynchrony between the two actuators may lead to force fighting and other adverse effects. Currently, commonly used synchronization control methods include mechanical synchronization, hydraulic synchronization, and position servo synchronization [18]. Mechanical synchronization features a simple structure and high reliability, but may suffer from jamming under large offset loads. Hydraulic synchronization achieves simultaneous motion among cylinders by controlling the oil supply flow for each cylinder through various synchronization control elements. Its synchronization accuracy depends heavily on relevant hydraulic elements and fluid properties, making it mainly suitable for applications with modest synchronization accuracy requirements. Position servo synchronization employs a closed-loop control mode with real-time detection and feedback of output values, which, to a large extent, eliminates or suppresses the influence of adverse factors and achieves high synchronization accuracy. Compared with the previous two methods, it offers better performance but requires a more complex and costly control loop. In recent years, position synchronization control systems have been extensively studied. Representative control methods include classical PID and its variants, but they show limited robustness under internal parameter changes or external disturbances. Therefore, multiple PID control technologies emerged, such as adaptive PID, fuzzy PID, intelligent integral PID, and nonlinear PID [19–23]. Aiming at slowly varying parameters of the controlled object, the adaptive control strategy automatically adjusts controller parameters based on real-time identification of object parameters [24–26]. Enhanced robust control schemes can be used to improve the system control performance, so as to mitigate uncertainties in system models [27,28]. To solve the problem of poor ability of the system to resist external disturbance and parameter change, an improved control strategy with a chattering-free sliding-mode variable structure has been designed to enhance the load disturbance resistance of the system [29–31]. Composite controllers that integrate artificial intelligence with automatic control have been developed to address complex nonlinear problems [32–36]. In view of uncertainties such as rapid parameter variations, a novel internal-model control approach based on the process mathematical model

for controller design can be adopted, which can effectively reduce external disturbance errors and simplify control signals [37–40].

Building upon prior research on control strategies and the first-generation heavy-duty unmanned wheeled platform developed by our team, this study addresses the limitations of conventional hydraulic steering systems in terms of weight, integration, energy efficiency, and maintainability. An overall approach that replaces the hydraulic system with a fully electrified actuation system is proposed, followed by the design, modeling, and simulation analysis of the full electrification solution. A compact direct-drive electro-mechanical actuator (DEMA) architecture with a reduced footprint is adopted as the core of the full electrification upgrade, laying a solid foundation for advancing the steering system and enabling system-level optimization of the heavy-duty unmanned wheeled platform.

This paper is organized as follows: Section 1 introduces the steering system employed in the first-generation heavy-duty unmanned wheeled platform developed by our team and outlines its limitations. Section 2 presents the design of steering systems based on single-channel and dual-channel DEMAs. Sections 3 and 4 focus on steering accuracy, response speed, and output consistency as key performance evaluation indicators, and on this basis, the control strategy for the single-channel DEMA-based steering system is optimized, the force-fighting issue in the dual-channel DEMA-based steering system is analyzed, and the corresponding synchronization control methods are investigated. Section 5 concludes the paper.

2. First-Generation Steering System Based on a Centralized Hydraulic Source

2.1. First-Generation Steering System Based on a Centralized Hydraulic Source

To meet the operational requirements of future heavy-duty unmanned wheeled platforms in special environments, our team developed a first-generation eight-wheel independently driven heavy-duty unmanned wheeled platform and verified its excellent environmental adaptability. The platform supports differential steering, Ackermann steering, and compound steering, demonstrating strong controllability, maneuverability, and terrain adaptability.

Figure 1 shows the steering system based on a centralized hydraulic source used in our first-generation heavy-duty unmanned wheeled platform. The system consists of the steering linkage, primary steering gear, secondary steering gear, hydraulic reservoir, hydraulic lines, and an electro-hydraulic pump. The first and second axles employ inclined double-wishbone steering suspensions, with their steering gears and linkages mounted relatively high on the inner front side of the vehicle body to provide enhanced protection. The third and fourth axles use unequal-length double-wishbone suspensions with large adjustable travel, suitable for negotiating extremely high geometric obstacles; the detailed suspension configuration is not repeated here.

During operation, the electro-hydraulic pump supplies hydraulic power, and the pressurized hydraulic fluid delivered by the pump is conveyed through hydraulic lines to drive the primary steering gear, thereby generating torque and displacement. The internal chambers of the primary and secondary steering gears are hydraulically connected, enabling synchronized motion of the secondary steering gear; the resulting action is transmitted through the steering linkage to effect vehicle steering. Because the primary and secondary steering gears share hydraulically connected internal chambers, this centralized hydraulic source-based steering system effectively prevents force fighting that may arise in dual-actuator systems.

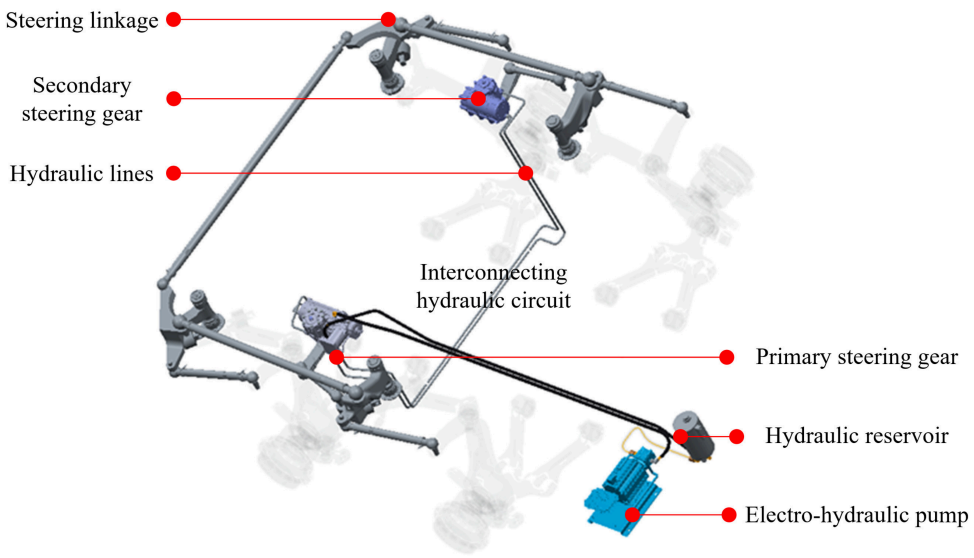


Figure 1. Architecture of the first-generation steering system based on a centralized hydraulic source.

2.2. Existing Problems and Full Electrification Upgrade

Figure 2 shows the major physical components of our first-generation steering system based on a centralized hydraulic source. Excluding the steering linkage, the steering system weighs approximately 150 kg.

Although this architecture effectively prevents force fighting in dual-drive systems and thereby ensures steering consistency under complex operating conditions, the two steering-gear assemblies are installed on opposite sides of the vehicle body and therefore require multiple hydraulic lines. This arrangement increases vehicle weight and is detrimental to lightweight design. In addition, the complex hydraulic piping compromises system maintainability, complicates overhauls, and hinders rapid wartime support. Long-distance fluid transmission and potential leakage reduce energy efficiency, and the extensive hydraulic network constrains system integration and modularization.

During the development and testing of our first-generation heavy-duty wheeled vehicle, it was found that although the centralized hydraulic suspension system could provide strong load-bearing support and static vehicle attitude adjustment, several significant challenges still remained:

(1) The hydraulic pipelines are distributed throughout the vehicle, interspersed between various sections and structural spaces, which not only greatly increases the integration difficulty of the system but also imposes significant restrictions on the overall vehicle structure design.
(2) The large hydraulic pipeline network, heavy valve groups and actuator components, and complex sealing requirements reduce system reliability and maintainability.
(3) The centralized hydraulic system experiences significant energy transmission losses during operation, especially in long-distance, high-complexity piping scenarios.
(4) The hydraulic system's dynamic response is constrained by the capabilities of the hydraulic pump station, making it difficult to achieve high-frequency and precise control, thus limiting the adaptive capability of the suspension system in complex battlefield environments.
(5) With the growing emphasis on lightweight, compactness, maintainability, and high mobility in modern special vehicles, the centralized hydraulic system gradually reveals many shortcomings.



Figure 2. Physical components of the first-generation steering system based on a centralized hydraulic source.

To address these drawbacks, this study proposes an optimized upgrade based on the existing steering system. The steering linkage is retained, while the primary and secondary steering gears are replaced with electro-mechanical actuators, and hydraulic components—including the hydraulic reservoir, hydraulic lines, and electro-hydraulic pump—are eliminated. Compared with a centralized hydraulic system, distributed electro-mechanical actuators implemented in a modular layout eliminate the extensive hydraulic network, significantly reducing both vehicle mass and spatial footprint. These actuators also provide higher energy efficiency, faster response, improved control precision, and better maintainability, thereby making the vehicle more integrated, modularized, and maintainable.

The heavy-duty unmanned wheeled platform requires the steering system to meet the following specifications: operating range $\geq \pm 40^{\circ}$, maximum output speed ≥ 6.7 rpm, rated output torque ≥ 6000 Nm, maximum output torque ≥ 8000 Nm, and no force fighting shall occur when multiple steering systems operate simultaneously.

As shown in Figure 3, the optimized steering system adopts a linear electro-mechanical actuator (EMA) combined with a rocker arm. When the steering system is centered, the actuator axis is perpendicular to the rocker arm, and the distance between the actuator tail shaft and the rotating shaft is 400 mm. The relevant parameters are described as follows:

(a) To achieve an operating range of at least $\pm 40^{\circ}$, the actuator is required to push or pull the rocker arm through the corresponding steering angle. Calculations indicate that, when the actuator output rod is at its minimum extension, the distance between the actuator tail shaft and the rotating shaft is 236 mm, with an equivalent lever arm of 147 mm; when the actuator output rod is at its maximum extension, this distance increases to 564 mm, with an equivalent lever arm of 207 mm.

(b) The required maximum output torque of the steering system is 8000 Nm. When the equivalent lever arm is 147 mm, the actuator experiences the most demanding condition. Assuming an end-effector efficiency of 98%, the maximum total output force shall be no less than 56 kN.

(c) The required maximum output speed of the steering system is at least 6.7 rpm. When the equivalent lever arm is 207 mm, the actuator experiences the most demanding condition. Accordingly, the actuator shall provide a maximum linear speed of no less than 146 mm/s. To satisfy the required steering angle, the effective stroke of the actuator shall be no less than 328 mm.

In summary, the linear EMA used in the steering system of the heavy-duty unmanned wheeled platform shall meet the following specifications: effective stroke ≥ 330 mm, maximum linear speed ≥ 150 mm/s, and maximum output force ≥ 56 kN.

EMAs that produce linear motion can be categorized into direct-drive and geared configurations, depending on how the motor interfaces with the motion-conversion mechanism. Direct-drive integrated EMAs can be further subdivided into three structural types according to their integration approach. Their compositions and comparative analyses have been detailed in the authors' previous publication [41] and are not repeated here.

Since this study focuses on the design and analysis of the steering system for heavy-duty unmanned wheeled platforms, a highly integrated, compact direct-drive electromechanical actuator (DEMA) architecture is selected as the design solution for the fully electrified steering system after comparing various structural configurations. In this design, the rotor of the servo motor and the nut of the planetary roller screw pair are integrated into a single unit. The motor drives the nut to rotate, and the screw consequently pushes the output rod, thereby producing linear motion and force.

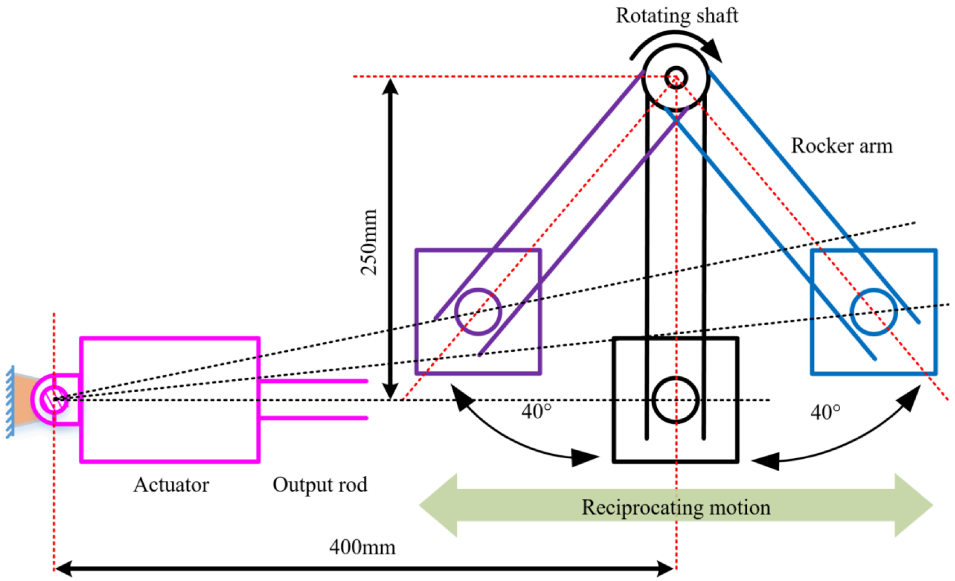


Figure 3. Schematic diagram of the fully electrified steering system.

3. Steering System Based on a Single-Channel DEMA

3.1. System Design

As analyzed earlier, the maximum linear output force required for the actuator is 56 kN. With a safety factor of 1.5, the reverse planetary roller screw pair RGTI30-4 manufactured by GSA (Lungern, Switzerland) can be selected. This planetary roller screw pair provides a dynamic load rating of 113.6 kN, a lead P_s of 4 mm, a pitch diameter d_s of 27 mm, and an effective stroke of 350 mm.

The key load-bearing components of the planetary roller screw pair are made of bearing steel GCr15, with a yield stress of 835 MPa. The allowable stress is taken as 210 MPa, with a modulus of elasticity Es of 2.1×10^5 MPa and a shear modulus Gs of 8.5×10^4 MPa.

Given that the maximum linear output force Femamax is 56 kN, the corresponding axial normal stress on the screw is:

$$\sigma_{0s} = \frac{4F_{emamax}}{\pi {d_s}^2} = 98 \text{ MPa} \quad (1)$$

With the efficiency of the planetary roller screw pair η_{prs} of 0.9, the torque applied to the screw is:

$$T_s = \frac{F_{emamax} P_s}{2\pi\eta_{prs}} = 39.7 \text{ Nm} \quad (2)$$

Thus, the equivalent stress on the screw is:

$$\sigma_{\text{screw}} = \sqrt{\sigma_{0s}^2 + 3\left(\frac{T_s}{0.2{d_s}^3}\right)^2} = 100 \text{ MPa} \quad (3)$$

This indicates that the screw strength meets the design requirements.

For a maximum linear output speed v_{max} of 150 mm/s, the corresponding maximum rotational speed of the screw pair is:

$$n_{so} = \frac{60 v_{max}}{P_s} = 2250 \text{ rpm} \quad (4)$$

The maximum torque T_s of the planetary roller screw pair under the maximum linear output force is:

$$T_s = \frac{F_{EMA} P_s}{2\pi \eta_{prs}} = 39.7 \text{ Nm} \quad (5)$$

Therefore, the input torque of the planetary roller screw pair should exceed 39.7 Nm, and the rotational speed should be greater than 2250 rpm. A Kollmorgen KBM-45X02B servo motor (Radford, VA, USA) can be selected to directly drive the screw pair to move. This servo motor provides a rated speed of 2350 rpm, a rated torque of 43.5 Nm, a rated power of 10.7 kW, and weighs 17.5 kg. The resulting steering system based on a single-channel DEMA offers the advantages of a compact axial structure and a high level of integration, with a total system weight of approximately 32 kg.

3.2. Performance Simulation Analysis

A position closed-loop simulation model of the DEMA was established in AMESim, as shown in Figure 4. The detailed modeling procedure and methodology for the DEMA dynamic performance simulation have been described in the authors' previous work [41] and are therefore not repeated here.

Given that feedforward control helps reduce steady-state errors and phase lag by providing compensation for the system before deviations occur, this study adopts a composite control strategy combining three-loop PID control with feedforward control to enhance the DEMA's responsiveness, stability, and accuracy.

The PID controller parameters used in this study were determined through multiple rounds of iterative tuning to achieve a balanced trade-off among response speed, tracking accuracy, overshoot suppression, and system stability under representative steering conditions. The final parameters were selected after repeated simulation verification under different operating scenarios.

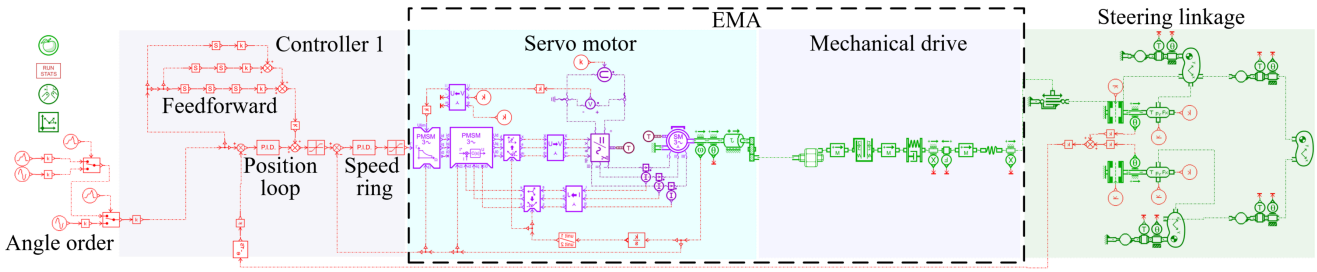


Figure 4. Simulation model of the steering system based on a single-channel DEMA.

A representative steering operating condition is selected for the simulation analysis of the heavy-duty special wheeled platform developed in this study. During the steering process, the vehicle steering system is subjected to a constant ground friction torque of

6000 Nm together with a random disturbance torque of ±500 Nm. The weight and stiffness of the steering linkage are determined according to the actual vehicle parameters. The simulation is conducted according to the following time sequence:

(a) 0–1 s: The vehicle travels straight on a flat road.
(b) 1–2 s: The steering angle changes from 0° to +30° within 1 s.
(c) 2–5 s: The steering angle is maintained at +30°.
(d) 5–6 s: The steering angle changes from +30° to 0° within 1 s.
(e) 6–9 s: The steering angle is maintained at 0°.
(f) 9–10 s: The steering angle changes from 0° to −30° within 1 s.
(g) 10–13 s: The steering angle is maintained at −30°.
(h) 13–14 s: The steering angle changes from −30° to 0° within 1 s, after which the vehicle resumes straight-line driving.

Figure 5 presents the simulation results, showing the tracking performance of the actual steering angle with respect to the commanded angle, as well as the time-varying curves of the actuator's linear output force and the ground friction torque during the steering process.

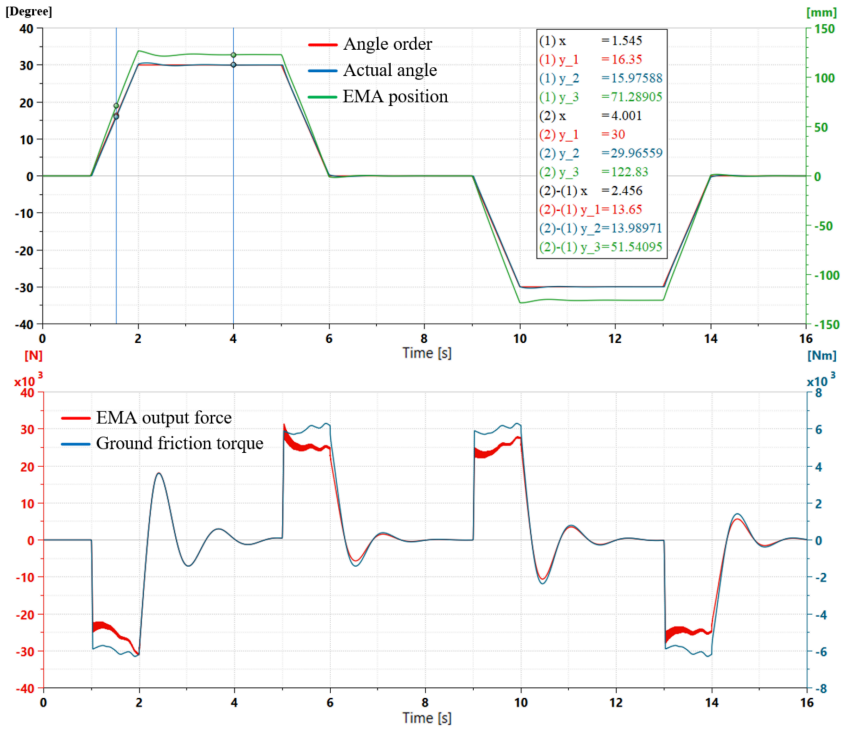


Figure 5. Simulation results of the steering system based on a single-channel DEMA.

(a) With the introduction of the composite control strategy, the vehicle's steering angle tracks the command signal with a fast response under a frictional resistance torque of 6000 ± 500 Nm. The system achieves high positioning and tracking accuracy, with an overshoot < 2%, a steady-state error < 0.1°, and a tracking error < 0.4°.
(b) The actuator's linear displacement corresponds well to the vehicle's steering angle. Within the steering range of ±30°, the actuator delivers a linear output displacement of approximately ±125 mm.
(c) The actuator's linear output force remains well synchronized with the ground frictional resistance torque. Even under large steering maneuvers, the system maintains a strong dynamic response, effectively ensuring high control accuracy.

Overall, the steering system based on a single-channel DEMA, equipped with the composite control strategy, demonstrates outstanding dynamic performance.

Although the single-channel DEMA demonstrates excellent dynamic performance as a steering actuator and effectively avoids force-fighting issues, preliminary design analysis shows that it is relatively large and heavy and places higher demands on motor power and thermal management. Therefore, two identical DEMAs are adopted to jointly provide the steering drive in place of the hydraulic system.

4. Steering System Based on a Dual-Channel DEMA

4.1. System Design

As analyzed earlier, the maximum output force of each actuator is 28 kN. With a safety factor of 1.5, the reverse planetary roller screw pair RGTI24-4 manufactured by GSA (Switzerland) can be selected. This planetary roller screw pair provides a dynamic load rating of 72 kN, a lead P_s of 4 mm, a pitch diameter d_s of 21 mm, and an effective stroke of 350 mm.

Given that the maximum linear output force F_{emamax} for each side is 28 kN, the corresponding axial normal stress on the screw is:

$$\sigma_{0s} = \frac{4F_{emamax}}{\pi {d_s}^2} = 80.9 \text{ MPa} \tag{6}$$

With the efficiency of the planetary roller screw pair η_{prs} of 0.9, the torque applied to the screw is:

$$T_s = \frac{F_{emamax} P_s}{2\pi\eta_{prs}} = 19.8 \text{ Nm} \tag{7}$$

Thus, the equivalent stress on the screw is:

$$\sigma_{screw} = \sqrt{\sigma_{0s}^2 + 3\left(\frac{T_s}{0.2{d_s}^3}\right)^2} = 83 \text{ MPa} \tag{8}$$

This indicates that the screw strength meets the design requirements.

For a maximum linear output speed v_{max} of 150 mm/s, the corresponding maximum rotational speed of the screw pair is:

$$n_{so} = \frac{60 v_{max}}{P_s} = 2250 \text{ rpm} \tag{9}$$

The maximum torque T_s of the planetary roller screw pair under the maximum linear output force is:

$$T_s = \frac{F_{EMA} P_s}{2\pi\eta_{prs}} = 19.8 \text{ Nm} \tag{10}$$

Therefore, for each screw pair, the input torque should exceed 19.8 Nm, and the rotational speed should be greater than 2250 rpm. A Kollmorgen KBM-35X04A servo motor can be selected to directly drive the screw pair to move. This servo motor provides a rated speed of 2800 rpm, a rated torque of 25.6 Nm, a rated power of 8.5 kW, and weighs 10.9 kg. The steering system based on a dual-channel DEMA has a total system weight of approximately 40 kg.

4.2. Performance Simulation Analysis

A simulation model of the system was likewise established in AMESim, as shown in Figure 6, with each channel independently producing linear force and displacement. The control parameters and mechanical parameters of the two channels are set to be identical.

The simulation analysis presented in this subsection is carried out using the same typical loading conditions and steering time sequence described in Section 3.2, thereby ensuring consistency for comparative evaluation.

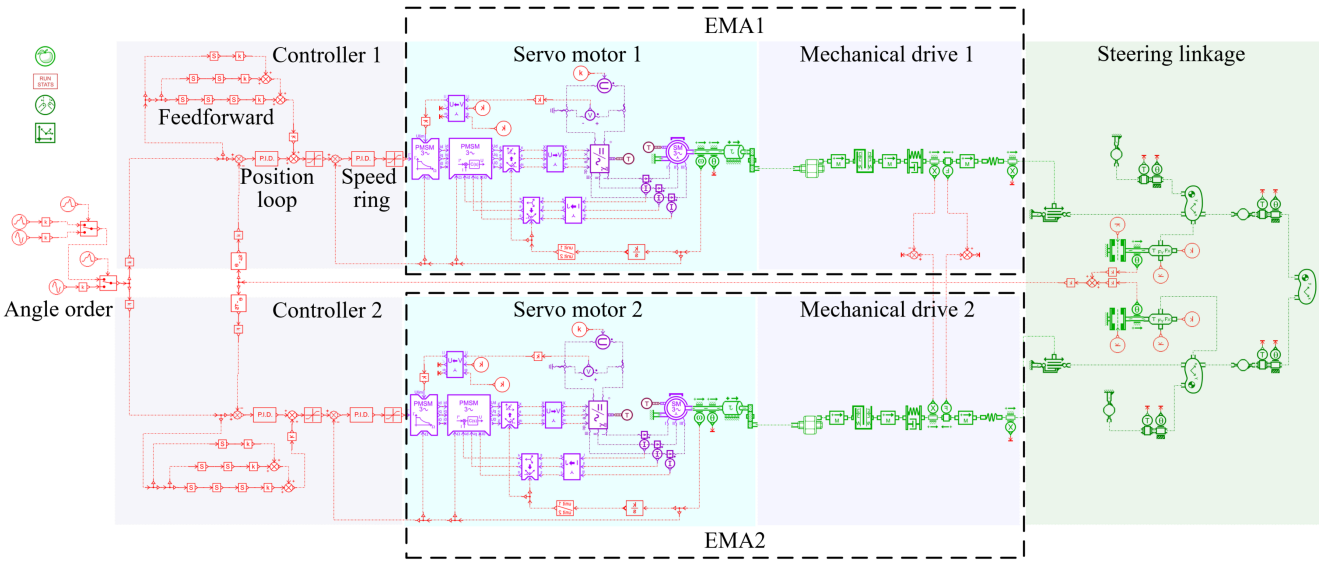


Figure 6. Simulation model of the steering system based on a dual-channel DEMA.

Figure 7 presents the simulation results under these conditions, showing the tracking performance of the actual steering angle with respect to the commanded angle, the relationship between each channel's linear output force and the resultant force, as well as the time-varying curves of the actuator linear output force, the ground friction torque, and the linear displacement of both channels during the steering process.

(a) For the steering system with two channels having identical parameters, the vehicle's steering angle rapidly tracks the command signal, achieving both high positioning and tracking accuracy. Its dynamic performance is nearly the same as that of the steering system based on a single-channel DEMA, with an overshoot < 2%, a steady-state error < 0.1°, and a tracking error < 0.4°.

(b) Throughout the steering process, the resultant force output by the two channels remains well synchronized with the variation of the ground frictional resistance torque, and the linear output forces of both channels remain identical.

(c) The actuator's linear displacement corresponds well to the vehicle's steering angle, and the linear displacement difference between the two channels remains within 0.01 mm during the steering process, indicating excellent synchronization and no force-fighting behavior.

As analyzed above, under ideal conditions, the steering system with dual channels having fully identical parameters exhibits excellent position-tracking performance. However, this is unrealistic in practical engineering applications, as inevitable differences exist between channels in measurement errors, joint stiffness, control parameters, and dynamic characteristics. Therefore, with the parameters of Channel 1 kept unchanged, the control system parameters and joint stiffness of Channel 2 are increased by 5% and 20%, respectively, relative to their original values, to simulate non-uniformity between channels. A simulation analysis is then conducted under the same time sequence.

When the parameter difference between the channels is 5%, the simulation results are shown in Figure 8.

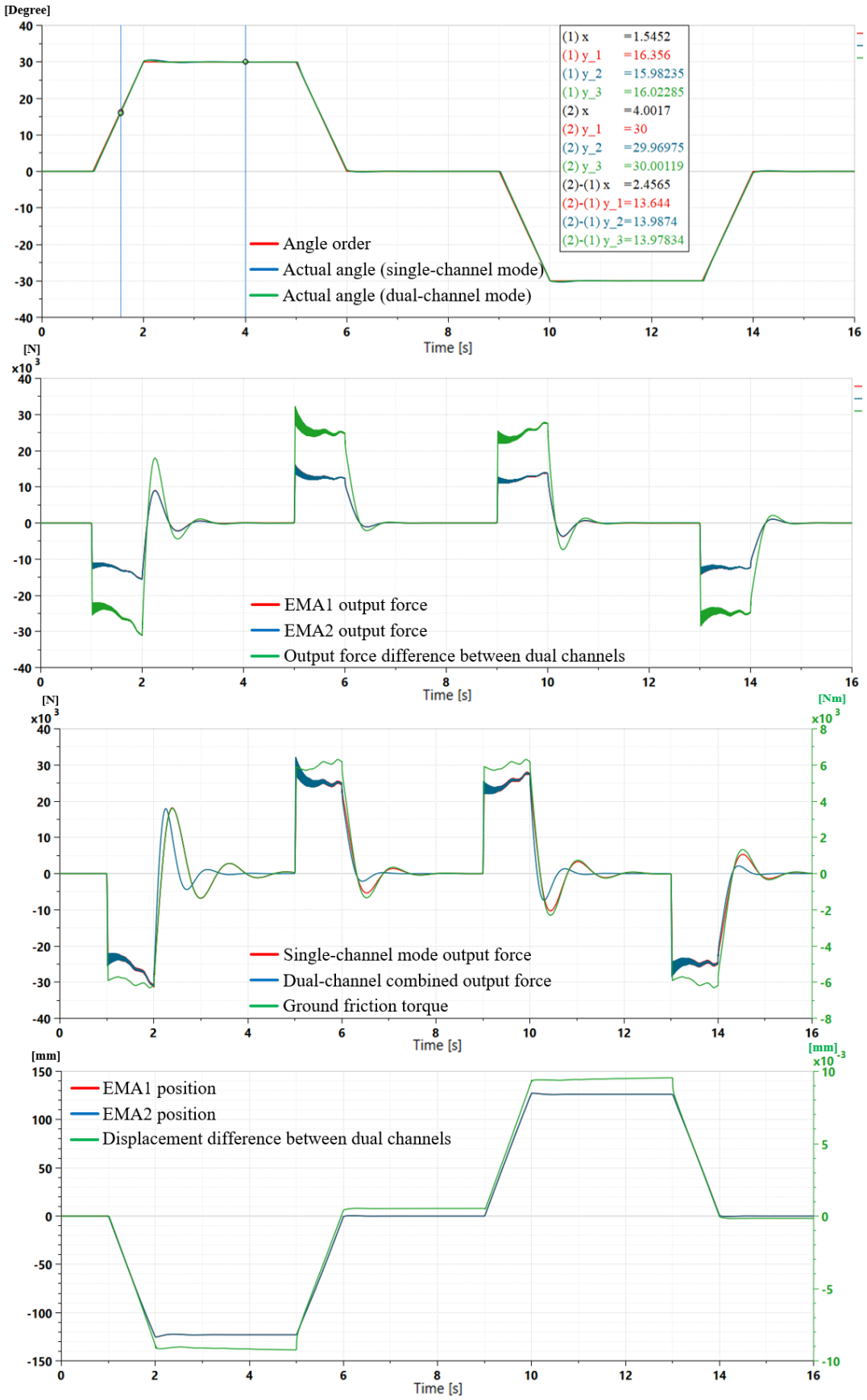


Figure 7. Simulation results of the steering system based on a dual-channel DEMA (identical parameters).

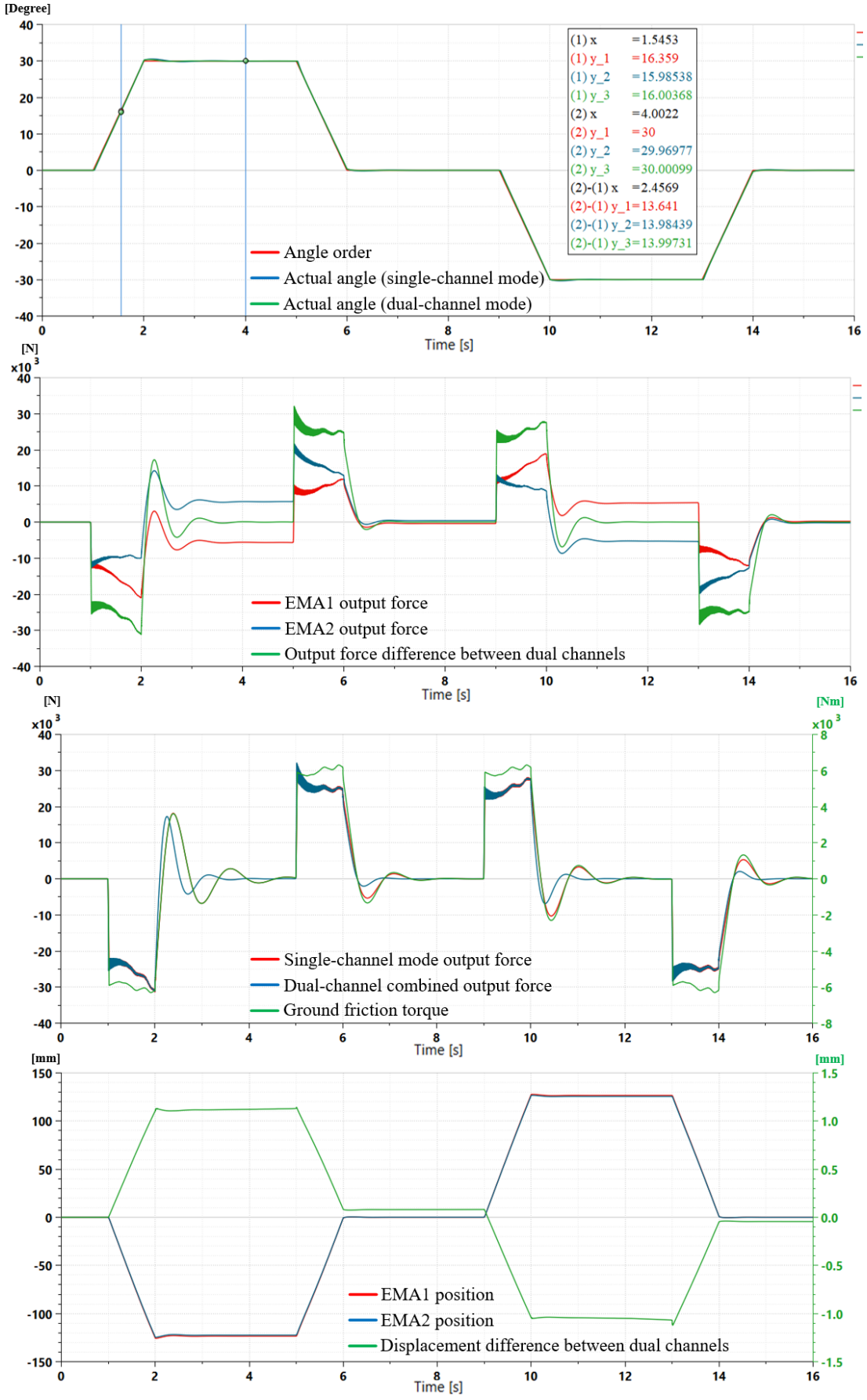


Figure 8. Simulation results of the steering system based on a dual-channel DEMA (5% parameter difference).

(a) The vehicle's steering angle continues to rapidly track the command signal, and the positioning and tracking accuracy remain high, with an overshoot < 2%, a steady-state error < 0.1°, and a tracking error < 0.4°.
(b) Throughout the steering process, the resultant force of the two channels remains well synchronized with the variation of the ground frictional resistance torque. However, due to inter-channel parameter differences, the two channels produce significantly different forces. During steering against the friction torque, one channel produces a noticeably larger force than the other, while during straight driving, the two channels produce equal and opposite forces, resulting in a force-fighting condition with a force magnitude of approximately 6 kN.
(c) The actuator's linear displacement corresponds well to the vehicle's steering angle, but due to force fighting, the linear displacement difference between the two channels during steering increases to approximately 1.1 mm, indicating poor synchronization.

When the parameter difference between the channels is 20%, the simulation results are shown in Figure 9.

(a) The vehicle's steering angle still rapidly tracks the command signal, and the positioning and tracking accuracy remain high, with an overshoot < 2%, a steady-state error < 0.1°, and a tracking error < 0.4°.
(b) Throughout the steering process, the resultant force of the two channels remains well synchronized with the variation of the ground frictional resistance torque. However, larger parameter differences cause a severe imbalance between the forces produced by the two channels. During steering against the friction torque, one channel needs to overcome not only the ground friction torque but also the opposing interference force induced by the other channel, indicating mutual resistance between actuators and resulting in significantly intensified force-fighting behavior.
(c) The actuator's linear displacement still corresponds well to the vehicle's steering angle, but the severe force fighting causes the linear displacement difference between the two channels to expand to 4.2 mm during steering, revealing very poor synchronization.

Overall, as the inter-channel parameter differences increase, the force-fighting behavior between the dual-channel DEMAs becomes significantly more severe. Even small inter-channel parameter differences may lead to noticeable opposing outputs and position asynchrony. Prolonged force fighting not only results in system energy loss and causes the actuators to operate in a mutually opposing, uncoordinated state, but also accelerates mechanical wear of components, induces fatigue in connection mechanisms, and causes substantial temperature rise in servo motors. These effects accelerate steering-system aging, reduce its service life, and compromise operational reliability. More critically, under high-frequency and high-intensity operating conditions, force fighting may further impair controller stability and system dynamic performance, potentially leading to response delays and output oscillations that directly affect vehicle steering precision and driving safety.

Therefore, to ensure high-performance and safe operation of the steering system under complex and varying conditions, a synchronization control strategy for dual-channel DEMAs should be designed to suppress or eliminate force-fighting behavior to the greatest extent possible, thereby effectively improving the safety, stability, and long-term durability of the steering system.

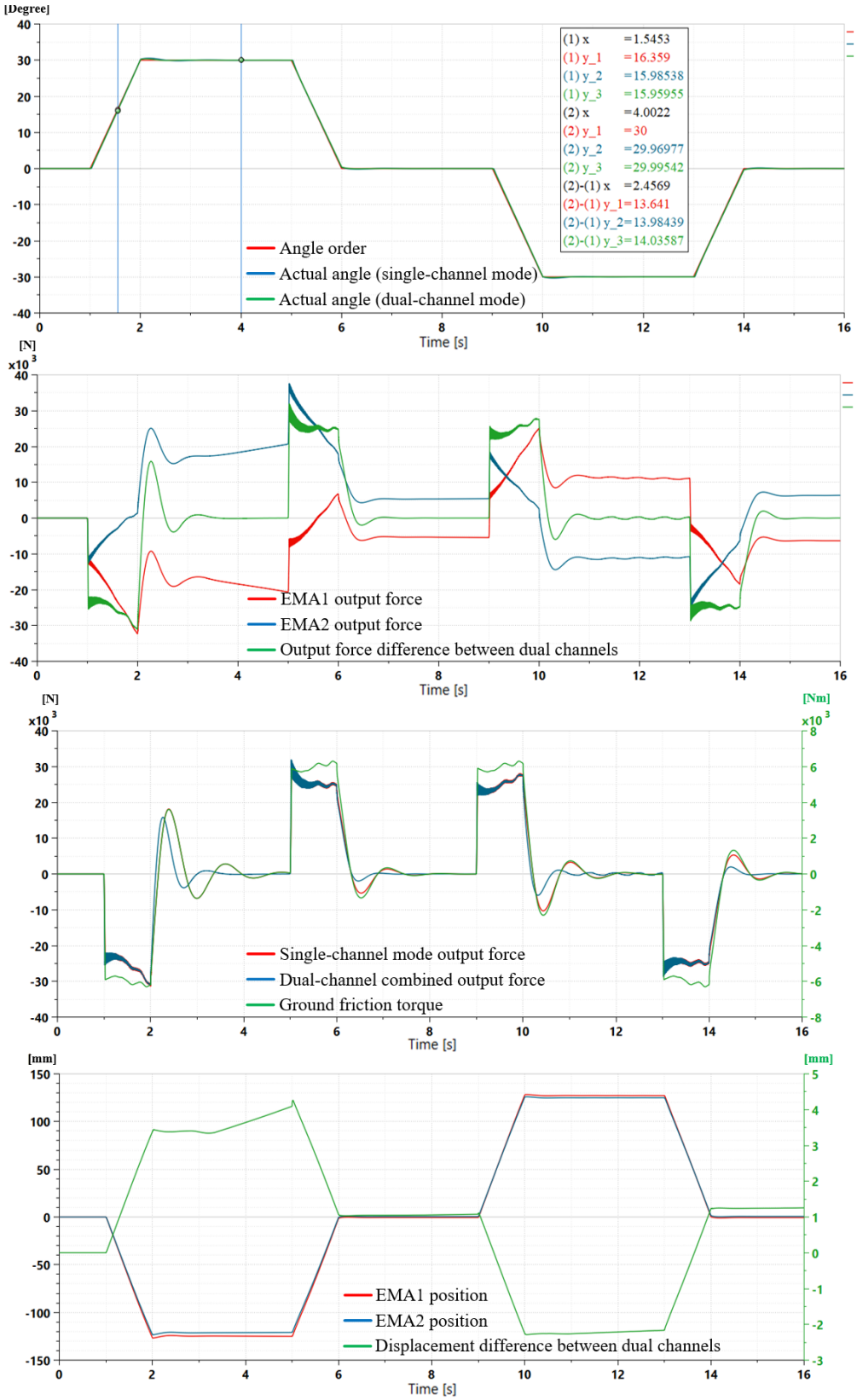


Figure 9. Simulation results of the steering system based on a dual-channel DEMA (20% parameter difference).

5. Synchronization Control Strategy for the Dual-Channel DEMA

To address the issues identified above, a primary–secondary position synchronization control strategy is adopted in this section. Channel 1 is designated as the primary channel, in which the original position servo system architecture is retained. The steering angle is

used as the closed-loop control objective to achieve accurate angle tracking. Channel 2 serves as the secondary channel and no longer directly tracks the steering angle. Instead, the actual displacement of Channel 1 is taken as the reference input for Channel 2, enabling precise following of the primary channel's motion state. The corresponding simulation model is shown in Figure 10.

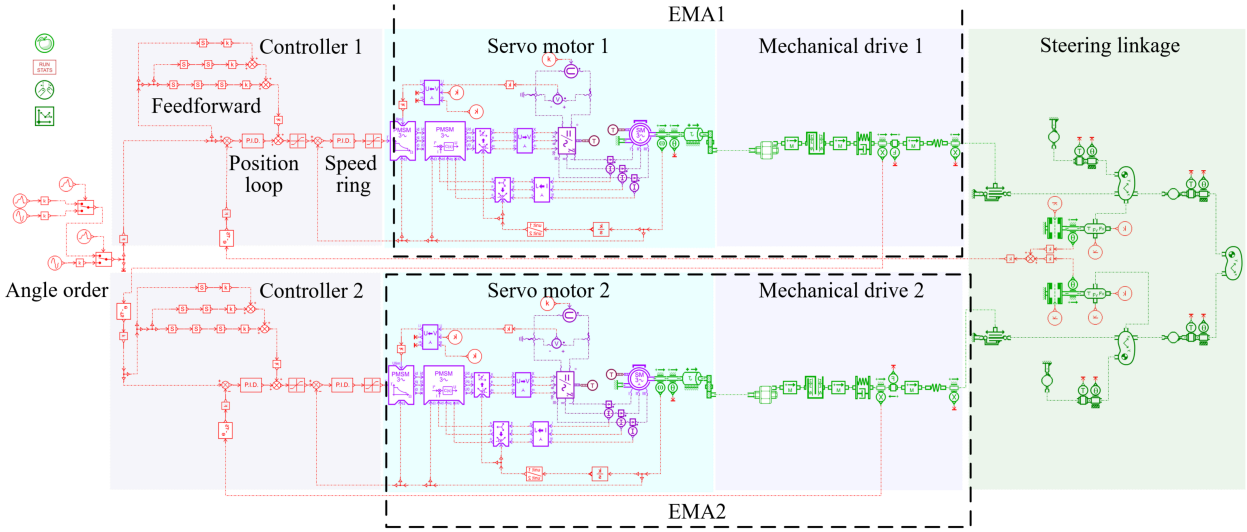


Figure 10. Simulation model of the steering system based on a dual-channel DEMA with the synchronization control strategy.

The effectiveness of the primary–secondary position synchronization control strategy depends not only on the excellent tracking performance of the primary channel, but also on whether the secondary channel can accurately follow the motion state of the primary channel. To ensure excellent tracking performance of the secondary channel, a composite control strategy combining three-loop PID control with feedforward control is applied to conduct a simulation analysis of the position-tracking performance of Channel 2.

The simulation results are shown in Figure 11. Channel 2 demonstrates fast and accurate responses to displacement commands, exhibiting excellent system dynamic performance. The steady-state error remains below 0.02 mm, and the tracking error in the steady-state phase is less than 0.1 mm. These results satisfy the requirements for high-precision synchronization control and provide a solid foundation for the synchronization control of the dual-channel steering system.

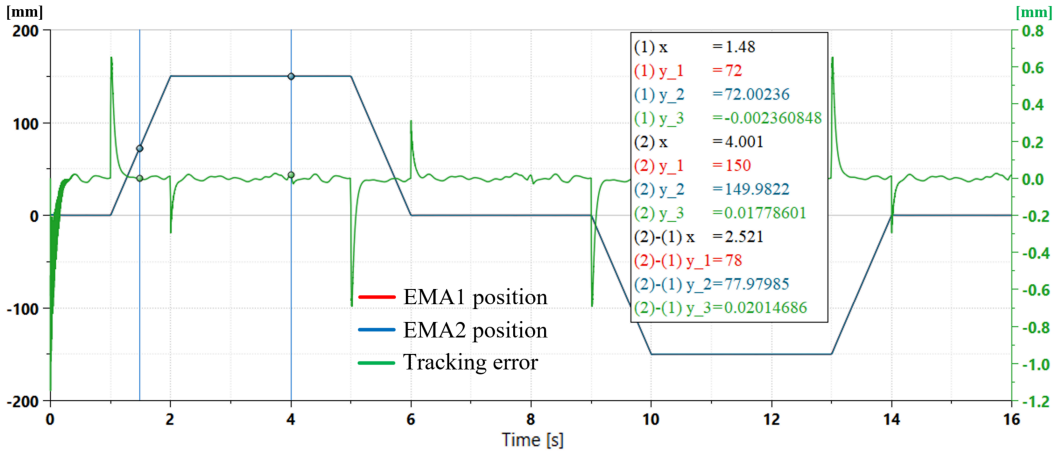


Figure 11. Simulation results of the position-tracking performance of Channel 2.

Consistent with the previous subsection, with the parameters of Channel 1 kept unchanged, the control system parameters and joint stiffness of Channel 2 are increased by 20%, respectively, relative to their original values. A simulation analysis is then conducted under the same time sequence, and the results are presented in Figure 12.

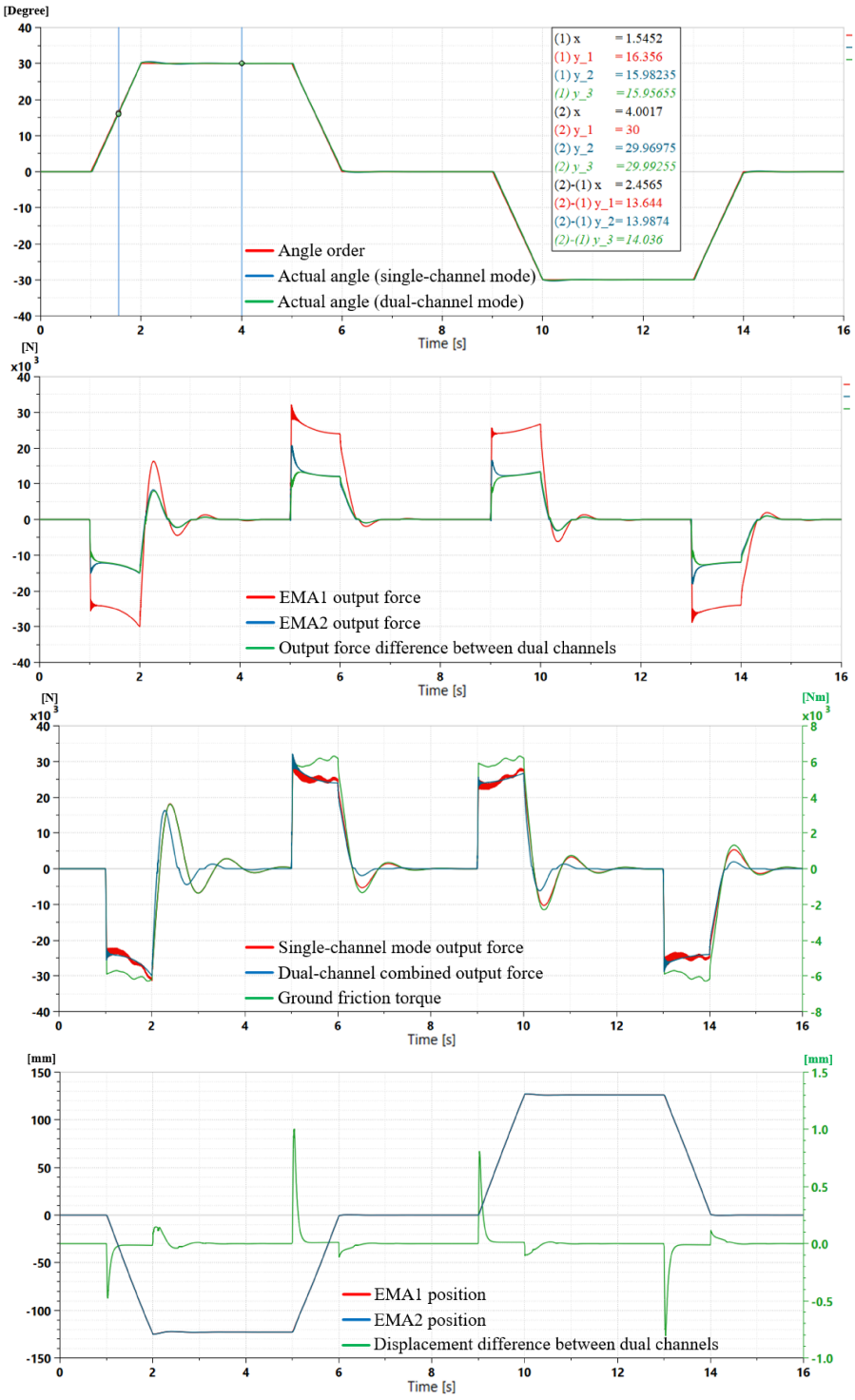


Figure 12. Simulation results of the steering system based on a dual-channel DEMA with the synchronization control strategy.

(a) The vehicle's steering angle rapidly tracks the command signal, achieving positioning and tracking accuracy nearly identical to that of the steering system based on a single-channel DEMA, with an overshoot < 2%, a steady-state error < 0.1°, and a tracking error < 0.4°.

(b) Throughout the steering process, the resultant force output in the dual-channel mode remains well synchronized with the variation of the ground frictional resistance torque. The transient force fluctuation occurring at the steering onset is significantly smaller than that observed in the single-channel mode. Except for a brief force-fighting behavior lasting approximately 0.2 s at the initial steering moment—caused by abrupt changes in steering velocity and acceleration—the output forces of Channel 1 and Channel 2 are identical, jointly counteracting the friction torque and exhibiting excellent force output consistency. If the steering angle and angular velocity transitions at the steering onset are further smoothed, force fighting can be almost completely eliminated.

(c) The actuator's linear displacement corresponds well to the vehicle's steering angle. A displacement difference of approximately 1 mm appears between the two channels only at the initial steering moment, which is also the primary cause of the short-duration force-fighting behavior.

In summary, by adopting the primary–secondary position synchronization control strategy and using the actual displacement of the primary channel as the reference input for the secondary channel, the dual-channel DEMA-based steering system is able to maintain high positioning and tracking accuracy even in the presence of inter-channel parameter differences, while achieving highly consistent force output and precise position synchronization.

6. Conclusions

The main contributions and conclusions of this study are summarized as follows.

(a) To address the limitations of the steering system based on a centralized hydraulic source, an integrated DEMA is adopted in this study to achieve a full electrification upgrade of both single-channel and dual-channel modes. This significantly improves system integration and maintainability, while reducing overall weight. As a result, the weight of the steering system after full electrification upgrade is reduced from 150 kg to 32 kg and 40 kg for single-channel and dual-channel modes, respectively.

(b) While retaining the original steering linkage, a steering system solution based on a single-channel DEMA is proposed. This system features small weight and size, low energy consumption, and a high degree of modularity. By introducing a composite control strategy that combines three-loop PID control with feedforward control, the position-tracking accuracy and dynamic responsiveness of the system are significantly improved. However, the single-channel mode still imposes relatively high requirements on motor power and thermal management.

(c) The proposed steering system based on a dual-channel DEMA effectively addresses the aforementioned issues. Furthermore, considering inter-channel parameter differences—such as measurement errors, joint stiffness, control parameters, and dynamic characteristics—which may lead to opposing outputs and position asynchrony, a primary–secondary position synchronization control strategy is proposed. This strategy ensures high positioning accuracy and excellent tracking performance of the vehicle during steering maneuvers, enabling highly consistent force output and precise position synchronization between the two channels.

This study is currently based on simulation analysis under typical operating conditions, and the effectiveness of the proposed all-electric steering system and control strategy still requires further verification through bench tests and vehicle experiments. Nevertheless, the simulation results provide a preliminary validation of the proposed method and demonstrate its potential for application in heavy-duty special wheeled vehicles. It should also be noted that the steering commands adopted in this study are simplified continuous reference signals intended to evaluate the synchronization characteristics and force-fighting behavior

of the proposed steering system under representative operating conditions. Future work will focus on system commissioning, PID fine tuning, discrete steering-command implementation, synchronization performance under continuously varying steering trajectories, bench-test validation, and experimental studies under real operating conditions.

Author Contributions: Conceptualization, S.Z., X.Y. and J.Z.; methodology, S.Z. and T.Q.; software, S.Z., J.W. and J.C.; validation, S.Z., X.Y. and J.Z.; formal analysis, S.Z., T.Q., J.W. and J.C.; investigation, X.Y. and J.Z.; resources, X.Y. and J.Z.; data curation, S.Z., T.Q., J.W. and J.C.; writing—original draft preparation, S.Z., T.Q., J.W. and J.C.; writing—review and editing, S.Z., X.Y. and J.Z.; supervision, X.Y. and J.Z.; project administration, X.Y. and J.Z.; funding acquisition, X.Y. and J.Z. All authors have read and agreed to the published version of the manuscript.

Funding: This research received no external funding.

Institutional Review Board Statement: Not applicable.

Informed Consent Statement: Not applicable.

Data Availability Statement: The dataset that supports the central findings of this study is directly available in this article. Additional data can be requested from the corresponding author.

Conflicts of Interest: The authors declare no conflict of interest.

Abbreviations

The following abbreviations are used in this manuscript:

DEMA	Direct-drive Electro-mechanical Actuator
EMA	Electro-mechanical Actuator

References

1. Chen, W.W.; Sun, X.W.; Wang, H.B. Extension coordinated control of automotive differential drive assisted steering system. *Sci. Sin. Technol.* **2017**, *47*, 324–335. [CrossRef]
2. Kou, F.R.; Chang, H.T.; Wang, Q.L.; Fang, B. Research on vehicle yaw stability analysis method based on state estimation. *J. Zhengzhou Univ. (Eng. Sci.)* **2025**, *46*, 105–110, 127. [CrossRef]
3. Li, Q.; Zhang, J.; Li, L.; Wang, X.; Zhang, B.; Ping, X. Coordination control of maneuverability and stability for four-wheel-independent-drive ev considering tire sideslip. *IEEE Trans. Transp. Electrif.* **2022**, *8*, 3111–3126. [CrossRef]
4. Huang, J.; Zhang, B.; Wang, H.; Zhao, L.; Jiang, P. Coordinated control and torque distribution of differential steering and anti-skid driving of distributed drive electric vehicles considering stability. *Proc. Inst. Mech. Eng. Part D J. Automob. Eng.* **2023**, *237*, 2780–2796. [CrossRef]
5. Choi, M.; Choi, S.B. Model predictive control for vehicle yaw stability with practical concerns. *IEEE Trans. Veh. Technol.* **2014**, *63*, 3539–3548. [CrossRef]
6. Fu, Q. Stability Control System Design for Distributed Drive Electric Bus. Master's Thesis, Zhejiang University, Hangzhou, China, 2021.
7. Zhao, Y.; Deng, H.; Li, Y.; Xu, H. Coordinated control of stability and economy based on torque distribution of distributed drive electric vehicles. *Proc. Inst. Mech. Eng. Part D J. Automob. Eng.* **2020**, *234*, 1792–1806. [CrossRef]
8. Hsu, Y.H.J.; Gerdes, J.C. Stabilization of a steer-by-wire vehicle at the limits of handling using feedback linearization. In Proceedings of the IMECE, Orlando, FL, USA, 5–11 November 2005. [CrossRef]
9. Zheng, H.; Zong, C.; Tian, C.; Zhu, T.; Dong, Y.; Yuan, D. Control algorithm for steer-by-wire system with ideal steering ratio. *J. Jilin Univ. (Eng. Technol. Ed.)* **2007**, *11*, 1229–1235. [CrossRef]
10. Wettergreen, D.; Tompkins, P.; Urmson, C.; Wagner, M.; Whittaker, W. Sun-synchronous robotic exploration: Technical description and field experimentation. *Int. J. Robot. Res.* **2005**, *24*, 3–30. [CrossRef]
11. Do, A.L.; Fauvel, F. Constrained LPV control for collision avoidance using mixed steering and differential braking. *Control Eng. Pract.* **2025**, *156*, 106214. [CrossRef]
12. von Vietinghoff, A.; Kiencke, U. Gain scheduling control for combined four-wheel steering and individual wheel braking. *IFAC Proc. Vol.* **2007**, *40*, 327–333. [CrossRef]
13. Wang, J. Study on Differential Drive Assist Steering Technology for Electric Vehicle with Independent-Motorized-Wheel-Drive. Ph.D. Thesis, Jilin University, Changchun, China, 2009.

14. Shen, Y.; Niu, T.; Liu, Z. Analysis of Energy Saving of Distributed-Drive Articulated Vehicle Based on Electro-HydraulicHybrid Steering System. *J. South China Univ. Technol. (Nat. Sci. Ed.)* **2022**, *50*, 84–92. [CrossRef]
15. Jin, L.; Tian, D.; Liu, Y. Coordinated Control of DDAS and ESC Systems for Electric Vehicle Driven by In-wheel Motors. *J. Mech. Eng.* **2018**, *54*, 160–169. [CrossRef]
16. Lu, S.; Xu, X.; Chen, L.; Wang, F.; Wang, W. Coordinated Control of Electronic Differential and Differential Assist Steering for Electric Vehicle Driven by In-wheel Motors. *J. Mech. Eng.* **2017**, *53*, 78–85. [CrossRef]
17. Xu, X.; Lu, S.; Chen, L.; Cai, Y.; Li, Y. Trajectory Tracking of Distributed-drive Self-driving Vehicle Based on Coordination Between Autonomous Steering and Differential Steering. *Automot. Eng.* **2018**, *40*, 475–481. [CrossRef]
18. Ren, F. The Discuss for Several Hydraulic Synchronization System. *Sichuan Metall.* **2007**, *29*, 44–47.
19. Wu, B.; Zou, D. Research on Intelligent Control System of Several Hydraulic Cylinders' Synchronous Operation. *Mach. Tool. Hydraul.* **2003**, *4*, 29–32+78.
20. Wang, R. Study of Fuzzy-PID Controller for the Electric-hydraulic Servo System. *Mech. Eng.* **2009**, *2*, 65–66.
21. Zhu, B.; Wu, R. Research for the fuzzy-immune-PID control of the electro-hydraulic servo system. *China Meas. Technol.* **2004**, *1*, 19–21.
22. Qiu, S.; Hu, D.; Hu, J. Application and Comparison of Three Control Algorithm in Hydraulic Synchronization System. *J. Chongqing Univ. Sci. Technol.* **2007**, *9*, 134–139. [CrossRef]
23. He, Q.; Zeng, Y. Hydraulic synchronization control based on fuzzy PID. *Mach. Electron.* **2001**, *1*, 13–16.
24. Liu, J.; Xu, Z.; Guo, Y. Synchronous Control of Hydraulic Cylinders. *Tech. Autom. Appl.* **2002**, *21*, 13–14.
25. Dang, K.; Zhou, R.; Lin, Y. Research on Robust Control Based on Model Reference Fuzzy Adaptive of an Electrohydraulic Position Servo System. *Mach. Tool. Hydraul.* **2003**, *4*, 208–209+71.
26. Pan, Y.; Wang, Q.; Yan, X. A novel method of model reference adaptive fuzzy control in hydraulic servo system. *Electr. Drive Autom.* **2007**, *29*, 5–8.
27. Sanada, K. A method of designing a robust force controller of a water-hydraulic servo system. *Proc. Inst. Mech. Eng. Part I J. Syst. Control Eng.* **2002**, *216*, 135–141. [CrossRef]
28. Hsia, T.C. A new technique for robust control of servo systems. *IEEE Trans. Ind. Electron.* **2003**, *36*, 1–7. [CrossRef]
29. Fang, Y.; Nie, Y.; Wang, Z. Adaptive Robust Variable Structure Control of Electro-hydraulic Servo Position System. *Comput. Simul.* **2006**, *23*, 149–154.
30. Liu, Q.; Wu, X.; Shi, Y. The Research of Integral Sliding Mode Adaptive Control in Electro-hydraulic Position Control System. *Mach. Tool. Hydraul.* **2008**, *36*, 126–129.
31. Yanada, H.; Shimahara, M. Sliding mode control of an electrohydraulic servo motor using a gain scheduling type observer and controller. *Proc. Inst. Mech. Eng. Part I J. Syst. Control Eng.* **1997**, *211*, 407–416. [CrossRef]
32. Zhao, J.; Sokola, M.A.; Edge, K.A. Self-learning control algorithm for an injection molding machine. In Proceedings of the 17th International Conference Hydraulics and Pneumatics, Ostrava, Czech Republic, 5–7 June 2001.
33. Shinada, M.; Kojima, E. Improvement of acceleration tracking accuracy of electro-hydraulic vibration testing machine. In Proceedings of the JFPS International Symposium on Fluid Power, Tokyo, Japan, 14–17 November 1999; pp. 631–636. [CrossRef]
34. Tewes, Q.; Harms, H.H. Fuzzy control for an electro-hydraulic load-sensing system. In Proceedings of the Fluid Power Systems, Ninth Bath International Fluid Power Workshop, Bath, UK, 9–11 September 1996.
35. Pai, K.R.; Shih, M.C. Multi-speed control of a hydraulic cylinder using self-tuning fuzzy control method. In Proceedings of the JFPS International Symposium on Fluid Power, Tokyo, Japan, 6–9 September 1999; pp. 99–104. [CrossRef]
36. Burton, R.T.; Ukrainetz, P.R.; Nikiforuk, E.H. Neural networks and hydraulic control: From simple to complex applications. *Proc. Inst. Mech. Eng. Part I J. Syst. Control Eng.* **1999**, *213*, 349–358. [CrossRef]
37. Zhao, Z.; Fang, Y.; Liu, K. Internal model control of electro-hydraulic servo systems. *Opto-Electron. Eng.* **2008**, *35*, 1–5.
38. Wang, J.; Wen, G.; Ji, J. Application of Robust Control in the Electro-hydraulic Loading System. *Mach. Tool. Hydraul.* **2008**, *36*, 100–103.
39. Zhao, Y.; Fang, Y.; Liu, K. Design of Robust Control Based on Internal Model Control for Electro-hydraulic Position Servo System. *Control Eng.* **2007**, *14*, 50–53. [CrossRef]
40. Yang, F.; Xu, J.; Guan, S.; Jiang, M. Research on Static Error Free Tracking Control of Electric-hydraulic Position Servo-system. *Hydraul. Pneum.* **2007**, *1*, 33–35.
41. Zheng, S.; Fu, Y.; Wang, D.; Zhang, W.; Pan, J. Investigations on system integration method and dynamic performance of electromechanical actuator. *Sci. Prog.* **2020**, *103*, 1–35. [CrossRef] [PubMed]

Disclaimer/Publisher's Note: The statements, opinions and data contained in all publications are solely those of the individual author(s) and contributor(s) and not of MDPI and/or the editor(s). MDPI and/or the editor(s) disclaim responsibility for any injury to people or property resulting from any ideas, methods, instructions or products referred to in the content.